Ocean Modelling 71 (2013) 102–113

Contents lists available at SciVerse ScienceDirect

Ocean Modelling

journal homepage: www.elsevier.com/locate/ocemod

Ocean wave transmission and reflection between two connecting viscoelastic ice covers: An approximate solution

Xin Zhao, Hayley H. Shen *

Department of Civil and Environmental Engineering, Clarkson University Potsdam, NY 13699, USA

ARTICLE INFO

Article history:
Available online 4 May 2013

Keywords:
Ice-covered oceans
Wave propagation
Viscoelastic
Transmission and reflection coefficients

ABSTRACT

An approximate solution for wave transmission and reflection between open water and a viscoelastic ice cover was developed earlier, in which both the water and the ice cover were treated as a continuum, each governed by its own equation of motion. The interface conditions included matching velocity and stresses between the two continua. The analysis provided a first step towards modeling the wave-in-ice climate on a geophysical scale, where properties of the ice cover change with time and location. In this study, we derive the wave transmission and reflection from one viscoelastic material to another. Only two modes of the dispersion relation are considered and the horizontal boundary conditions are approximated by matching the mean values. The reflection and transmission coefficients are first determined for simplified cases to compare with earlier theories. All results show reasonable agreement when the same physical parameters are used. Behaviors of the transmission and reflection coefficients are then obtained for a range of viscoelastic covers. A mode switching phenomenon with increasing ice shear modulus is found. This phenomenon was pointed out in the study of wave propagation from open water to a viscoelastic cover. For two connecting viscoelastic covers, such mode switching is found to terminate with increasing viscosity. Together with an earlier investigation of wave dispersion in a viscoelastic ice cover, the present study provides a way to implement theoretical results in a numerical model for wave propagation through a heterogeneous ice cover. In discretizing a continuously changing ice cover over the geophysical scale, on top of the energy advection, energy transmission between computational cells due to the heterogeneity can be estimated using the present method, while the attenuation and wave speed within each cell are from the previously obtained dispersion relation. In addition, on floe scales, this study provides a way to determine wave scattering from an ice floe imbedded in grease or brash ice.

1. Introduction

As part of the climate change scenario, global wind and wave heights have increased in the past two decades (Young et al., 2011). In particular, wave conditions in the Arctic have intensified as the ice cover shrinks (Francis et al., 2011). The pressure for better wave models in the Arctic increases as the economic and environmental interests in this region rise. At present, existing operational wave models can only treat ice covers crudely. For example, in WAVEWATCH III, an ice cover is considered as a stepwise filter in such a way that the fraction of wave energy flux at any location varies linearly between 0 and 1, with two threshold values controlling this stepwise linear variation, both are related to the local ice concentration (Tolman, 2003). The group velocity is assumed unaltered from the open water condition. This model was established at a time when the only available ice parameter was the ice concentration and the wave conditions in the Arctic were not of great concern. In reality, waves can penetrate into ice-covered seas over a very long distance. Along its passage, wave energy is dissipated by the ice field. The attenuation rate depends on the wave period, ice concentration, thickness and floe size distribution (Wadhams et al., 1988; Squire et al., 1995; Squire, 2007). In turn, waves may break the ice floes and further complicate their interactive nature (Dumont et al., 2011). In addition, wind-wave generation may be modified greatly in the presence of a partial ice cover (Masson and Leblond, 1989; Perrie and Hu, 1996). Integrating ice effects into wave models will advance wave predictions in ice-covered seas. With better remote sensing capabilities, information on ice conditions will improve. Wave models that can utilize this improvement need to be developed.

In an earlier study, Wang and Shen (2010, 2011) proposed a linear viscoelastic model to represent a general ice cover. This continuum-based approach allowed the water and the overlying ice cover to each deform internally according to its own material properties. The requirement of matching interfacial conditions determine both the dispersion relation of the wave that travels into

* Corresponding author. Tel./fax: +1 315 268 7985.
E-mail address: hhshen@clarkson.edu (H.H. Shen).

1463-5003/$ - see front matter © 2013 Elsevier Ltd. All rights reserved.
http://dx.doi.org/10.1016/j.ocemod.2013.04.002

the ice cover (Wang and Shen, 2010) and the reflection and transmission of wave energy from open water into an ice cover (Wang and Shen, 2011). The dispersion relation was shown to converge to three types of existing models under respective limiting conditions: the mass loading (Peters, 1950; Weitz and Keller, 1950), thin elastic plate (Wadhams, 1973a), and pure viscous layer (Keller, 1998). For general viscoelastic ice layer of finite thickness, many coexisting modes for the transmitted wave were possible. The series of coexisting modes were truncated to include the first two closest to the open water mode to determine the reflection and transmission properties from open water to an ice cover (Wang and Shen, 2011). It was found that each of these two modes became dominant in an ice covers with either low or high shear modulus, respectively. For intermediate shear modulus, both modes could play a role. The results of this approximate solution were shown to be close to the exact solutions available at the thin elastic plate limit for high shear modulus cases.

In the present study, we extend the previous work to investigate wave propagation from one viscoelastic cover into another. The motivation for this study is evident: to mathematically model the wave propagation over a large expanse with varying physical conditions, a numerical method is required. All numerical methods discretize the computational domain into finite size "cells". Within each cell, average properties of variables are considered. A continuously varying ice cover is thus discretized into cells of constant thickness and material properties within each cell and abrupt changes between cells. Wave damping mechanisms contribute to the sink term within each cell. At the boundary between neighboring cells wave flux contributes to the energy transport. Both damping and flux terms are required for any numerical wave models. Transmission and reflection at cell boundaries are in fact part of the cumulative results of this process that take place at the floe scale, where all discontinuities contribute to this process. The types of floe scale discontinuities and their scattering properties are shown in Bennetts and Squire (2012). Part of the cumulative results is accounted for in the wave attenuation due to the average properties of the ice within the cell. The part due to the gradient of the ice properties within the cell is accounted for at the cell boundary. These two processes are shown schematically in Fig. 1, where the sink term has been studied as part of the dispersion relation in Wang and Shen (2010). The flux term is the focus of the present study.

Incidentally, the same analysis provided herein may also help to expand floe scale investigations. Wave scattering theory developed by Wadhams (1973a,b) and later extensively studied by Squire and colleagues (Squire, 2007; Bennetts and Squire, 2009, 2012; Bennetts et al., 2010) considered ice floes dispersed in open water. The present work may expand these theories to situations of ice floes imbedded in a grease or brash ice field. These two different types of ice covers are shown in Fig. 2.

To determine the flux between two adjacent ice covers with different viscoelastic properties, in this study we will use the same approximate approach as given in Wang and Shen (2011). We will consider two leading modes only to determine the partition of energy of each mode for a linear monochromatic gravity wave. Our treatment of the horizontal boundary conditions will also follow the same approximation method. The organization of this paper is as follows. Section 2 briefly outlines the theoretical formulation of the viscoelastic model. In Section 3, the approximation method is presented. Section 4 gives the result of special cases to compare with previous studies for pure elastic ice covers. Section 5 discusses the characteristics of the reflection and transmission for a range of viscoelastic parameters. The summary and conclusions are given in Sections 6 and 7 respectively. A linear wave regime is assumed in this study.

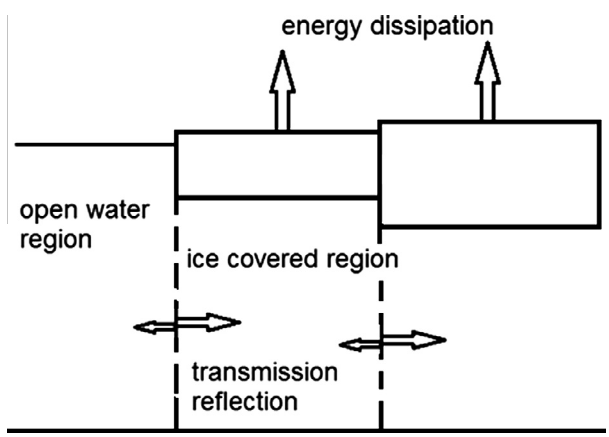

Fig. 1. Schematic of a discretized field of wave propagation into a continuous heterogeneous ice cover.

Fig. 2. (Left) A photo of a broken up ice cover interspersed in open water. The narrow range of size distribution suggests a wave induced breakage. (Credit: Vernon Squire). (Right) A photo of ice floes interspersed with pancake ice. (Credit: Don Perovich).

2. The theoretical formulation

2.1. Definition of the domain

The problem to be analyzed is two dimensional. The two ice covers are assumed to be fully submerged. This assumption is based on the results from Williams and Porter (2009), where it is shown that the draft of a floating ice cover affects the wave transmission and reflection. The small amount of ice cover exposed in air is ignored in this study. The coordinate system used in this study is shown in Fig. 3. The x direction is aligned with the incoming wave direction, and the z direction is opposite to gravity. The origin is set at the top of the ice cover right between the two ice regions. As shown in Fig. 3, there are four regions: ice regions 1 and 3; water regions 2 and 4. A monochromatic wave propagates from left to right. The ice thickness for regions 1 and 3 are h_1 and h_3, respectively. The total depth of the domain is H.

2.2. Governing equation

For the ice cover, we use a Voigt viscoelastic continuum model shown below (Wang and Shen, 2011):

$$\tau_{mn} = -p\delta_{mn} + 2GS_{mn} + 2\rho_{ice}\nu\dot{S}_{mn}, \tag{1}$$

where ρ_{ice} is the density of the ice layer; τ_{mn}, S_{mn} and $\dot{S}_{mn}$ represent the stress tensor, the strain tensor and the strain rate tensor, respectively; m and n represent x or z; G and ν are the effective shear modulus and the effective kinematic viscosity of the ice layer, respectively; p is the pressure and δ_{mn} the Kronecker delta. The equation of motion is

$$\frac{\partial \mathbf{U}_i}{\partial t} = -\frac{1}{\rho_{ice}}\nabla p_i + \nu_{ei}\nabla^2\mathbf{U}_i + \mathbf{g} \quad i = 1, 3, \tag{2}$$

where $\mathbf{U}_i$ is the velocity vector, $\mathbf{g}$ the gravitational acceleration, and ν_{ei} the viscoelastic parameter:

$$\nu_{ei} = \nu_i + iG_i/\rho_{ice}\omega \quad i = 1, 3. \tag{3}$$

In which, ν_i and G_i are the effective parameters in each respective region i, and ω is the angular frequency of the incoming wave. Using the decomposition with potential function φ_i and stream function ψ_i for the velocity (Lamb, 1932),

$$\mathbf{U}_i = -\nabla\varphi_i + \nabla \times (0, \psi_i, 0) \quad i = 1, 3, \tag{4}$$

we obtain

$$\nabla^2\varphi_i = 0, \tag{5}$$

$$\frac{\partial \psi_i}{\partial t} - \nu_{ei}\nabla^2\psi_i = 0, \tag{6}$$

$$\frac{\partial \varphi_i}{\partial t} - \frac{p_i}{\rho_{ice}} - \Phi = 0 \quad i = 1, 3. \tag{7}$$

Here, $\Phi = gz$ is the gravitational potential.

For water regions 2 and 4, we assume an inviscid fluid. The governing equations are

$$\frac{\partial \mathbf{U}_i}{\partial t} = -\frac{1}{\rho_{water}}\nabla p_i + \mathbf{g}, \tag{8}$$

$$\nabla^2\varphi_i = 0, \tag{9}$$

$$\frac{\partial \varphi_i}{\partial t} - \frac{p_i}{\rho_{water}} - \Phi = 0 \quad i = 2, 4. \tag{10}$$

The water velocity is related to the velocity potential only:

$$\mathbf{U}_i = -\nabla\varphi_i \quad i = 2, 4. \tag{11}$$

In terms of the Fourier modes, the solution for a sinusoidal wave with two modes can be written as (Wang and Shen, 2011)

$$\varphi_i(x, z, t) = \sum_{n=1}^{2}(A_i(n)\cosh k_i(n)z + B_i(n)\sinh k_i(n)z)e^{ik_i(n)x}e^{-i\omega t}, \tag{12}$$

$$\psi_i(x, z, t) = \sum_{n=1}^{2}(C_i(n)\cosh\alpha_i(n)z + D_i(n)\sinh\alpha_i(n)z)e^{ik_i(n)x}e^{-i\omega t} \tag{13}$$

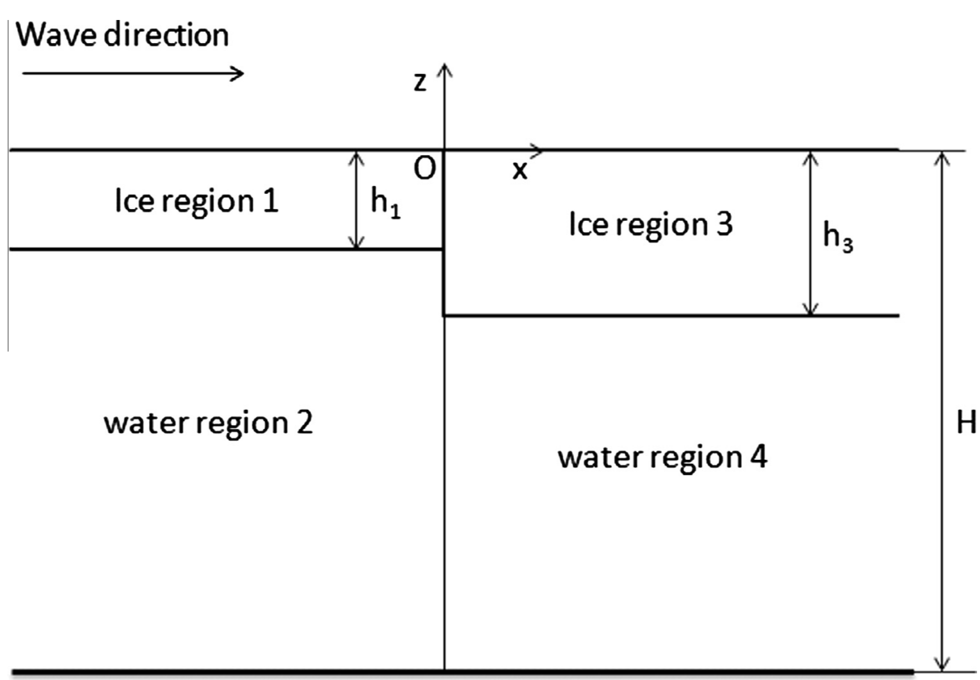

Fig. 3. Schematic of the coordinate frame of the problem.

for the ice region $i = 1, 3$ and $-h_i \leqslant z \leqslant 0$, and

$$\varphi_i(x,z,t) = \sum_{n=1}^{2} E_i(n) \cosh k_i(n)(z+H) e^{ik_i(n)x} e^{-i\omega t} \tag{14}$$

for the water region $i = 2, 4$ and $-H \leqslant z \leqslant -h_i$. The coefficients $A_i(n)$, $B_i(n)$, $C_i(n)$, $D_i(n)$, and $E_i(n)$ are complex constants. As shown in Appendix B the solution of these constants can be obtained by using the vertical boundary conditions described in Section 2.3. In the above, $\alpha_i^2(n) = k_i^2(n) - i\omega/v_{ei}$ for $i = 1, 3$ and $n = 1, 2$ from Eq. (6). Here $k_i(n)$ is the wave number for each ice-covered region.

2.3. Boundary conditions in the vertical direction

In the vertical direction, there are three boundaries. From top to bottom: the first boundary is between the air and the ice cover, the second is between the ice cover and the water underneath, and the third is between the water and the sea floor. Stress-free conditions apply between the air and the ice cover,

$$\tau_{xzi}(x,0) = 0, \quad \tau_{zzi}(x,0) = 0, \quad i = 1,3. \tag{15}$$

The stresses and vertical velocities between the ice and the water must be equal,

$$\tau_{xz1}(x,-h_1) = \tau_{xz3}(x,-h_3) = 0, \tag{16}$$

$$\tau_{zz1}(x,-h_1) = \tau_{zz2}(x,-h_1); \quad \tau_{zz3}(x,-h_3) = \tau_{zz4}(x,-h_3), \tag{17}$$

$$w_1(x,-h_1) = w_2(x,-h_1); \quad w_3(x,-h_3) = w_4(x,-h_3). \tag{18}$$

The third boundary condition requires zero vertical velocity at the sea floor, which is guaranteed by Eq. (14). Both the left and right side of the domain are governed by the same set of governing equations and boundary conditions in the vertical direction. The dispersion relation for either side of the ice-covered region has been obtained in Wang and Shen (2010) as shown below.

$$\omega^2 = \left(1 + \frac{\rho_{ice}}{\rho_{water}} \frac{g^2 k^2 S_k S_\alpha - (N^4 + 16k^6\alpha^2 v_e^4) S_k S_\alpha - 8k^3 \alpha v_e^2 N^2 (C_\alpha C_k - 1)}{gk(4k^3 \alpha v_e^2 S_k C_\alpha + N^2 S_\alpha C_k - gk S_k S_\alpha)}\right) gk \tanh kH, \tag{19}$$

where $S_k = \sinh kh$, $S_\alpha = \sinh \alpha h$, $C_k = \cosh kh$, $C_k = \cosh kh$, $N = \omega + 2ik^2 v_e$. The viscoelastic model gives a general dispersion relation that has been shown to reduce to previously established three models under limiting conditions: the mass loading, the thin elastic plate, and the viscous layer model. The real part of $k = \kappa + iq$ denotes the wavelength under the ice cover and the imaginary part denotes the attenuation. The dispersion relation was shown to have infinite solutions. The two closest to the open water solution were chosen to create an approximate solution for the wave propagation between open water and a general viscoelastic ice cover (Wang and Shen 2011).

2.4. Boundary conditions in the horizontal direction

We now proceed to determine the horizontal boundary conditions between two different viscoelastic regions. In the horizontal direction between the two ice regions and the two water regions, we need to match the displacements, velocities, and stresses.

2.4.1. Water–water interface

The boundary condition between water regions 2 and 4 includes continuity of the potential and the horizontal velocity

$$\varphi_2(0,z) = \varphi_4(0,z), \quad -H < z < -h_3, \tag{20}$$

$$\frac{\partial \varphi_2(0,z)}{\partial x} = \frac{\partial \varphi_4(0,z)}{\partial x}, \quad -H < z < -h_3. \tag{21}$$

2.4.2. Water–ice interface

For the time being we assume $h_1 < h_3$, the same analysis may be applied to other cases. Between water region 2 and ice region 3, the kinematic condition is

$$u_2(0,z) = u_3(0,z), \quad -h_3 < z < -h_1. \tag{22}$$

Likewise, the dynamical boundary condition is

$$\tau_{xx2}(0,z) = \tau_{xx3}(0,z), \quad -h_3 < z < -h_1. \tag{23}$$

These two conditions are the same as in Wang and Shen (2011) for wave propagating from open water to an ice covered region. Additionally, we also include the continuity condition of shear stress at the interface:

$$\tau_{xz3}(0,z) = 0, \quad -h_3 < z < -h_1. \tag{24}$$

2.4.3. Ice–ice interface

Between ice region 1 and ice region 3, we use the continuity conditions of horizontal and vertical velocities, and normal and shear stresses:

$$u_1(0,z) = u_3(0,z), \quad -h_1 < z < 0, \tag{25}$$

$$w_1(0,z) = w_3(0,z), \quad -h_1 < z < 0, \tag{26}$$

$$\tau_{xx1}(0,z) = \tau_{xx3}(0,z), \quad -h_1 < z < 0, \tag{27}$$

$$\tau_{xz1}(0,z) = \tau_{xz3}(0,z), \quad -h_1 < z < 0. \tag{28}$$

2.4.4. Summary of boundary conditions

The above nine equations, Eqs. (20)–(28), will be used to determine the transmission and reflection coefficients for a given wave. If freeboard is modeled instead of the current full submergence assumption, we will also need to include the stress free conditions over the exposed air–ice interface at $x = 0$.

$$\tau_{xx}(0,z) = \tau_{xz}(0,z) = 0, \quad 0 < z < h_{\text{freeboard}} \tag{29}$$

These conditions are ignored at present.

In a previous study of wave propagation from one ice cover to another, Barrett and Squire (1996) represented both ice covers as thin elastic plates each with its own properties. Their boundary conditions between the two ice covers are the continuity of the vertical displacement, slope, bending moment and shear force. The integral of normal stress distribution is the bending moment and the integral of shear stress distribution is the shear force, hence the boundary conditions used in Barrett and Squire (1996) for a thin plate correspond one to one with our continuum boundary conditions.

Eqs. (20)–(28) represent nine sets of infinite equations which cannot be solved exactly. Instead, a least-square method based on the variational method is commonly used to minimize the error function (see Fox and Squire, 1990, 1994):

$$\varepsilon = \sum_{n=1}^{9} \lambda_n \int_{l_n}^{u_n} |F_b^n - F_a^n|^2 dz, \tag{30}$$

where λ_n are the Lagrange multipliers, l_n and u_n are the bounds of the domain where the matching conditions are applied, F_a^n, F_b^n are the corresponding functions that must be matched at two sides, a and b, of each boundary. However, in this study we use a simpler but less accurate approach. We adopt the same approximation as in Wang and Shen (2011), in keeping with the fact that we only include two of the multiple modes in the dispersion relation Eq. (19). The boundary conditions are approximated by setting the integrals of the required conditions to zero. In this way, we do not minimize the error but require the mean values of both sides of the respective functions be the same. By comparing with the limiting case of pure elastic ice covers, we will get a sense of how well this approximation works.

To summarize, the following equations are the approximated nine horizontal boundary conditions in terms of the potential and stream functions. The derivation of the normal and shear stresses in terms of the potential and stream functions is given in Appendix A.

$$\int_{-H}^{-h_3} \varphi_2(0,z)dz = \int_{-H}^{-h_3} \varphi_4(0,z)dz, \tag{31}$$

$$\int_{-H}^{-h_3} \frac{\partial \varphi_2(0,z)}{\partial x}dz = \int_{-H}^{-h_3} \frac{\partial \varphi_4(0,z)}{\partial x}dz, \tag{32}$$

$$\int_{-h_1}^{0} \left(-\frac{\partial \varphi_1(0,z)}{\partial x} - \frac{\partial \psi_1(0,z)}{\partial z}\right)dz = \int_{-h_1}^{0} \left(-\frac{\partial \varphi_3(0,z)}{\partial x} - \frac{\partial \psi_3(0,z)}{\partial z}\right)dz; \tag{33}$$

$$\int_{-h_1}^{0} \left(-\frac{\partial \varphi_1(0,z)}{\partial z} + \frac{\partial \psi_1(0,z)}{\partial x}\right)dz = \int_{-h_1}^{0} \left(-\frac{\partial \varphi_3(0,z)}{\partial z} + \frac{\partial \psi_3(0,z)}{\partial x}\right)dz, \tag{34}$$

$$\int_{-h_1}^{0} \left[i\omega\rho_{ice}\varphi_1(0,z) + 2\rho_{ice}\nu_{e1}\left(-\frac{\partial^2 \varphi_1(0,z)}{\partial x^2} - \frac{\partial^2 \psi_1(0,z)}{\partial x \partial z}\right)\right]dz = \int_{-h_1}^{0} \left[i\omega\rho_{ice}\varphi_3(0,z) + 2\rho_{ice}\nu_{e3}\left(-\frac{\partial^2 \varphi_3(0,z)}{\partial x^2} - \frac{\partial^2 \psi_3(0,z)}{\partial x \partial z}\right)\right]dz, \tag{35}$$

$$\int_{-h_3}^{-h_1} \left(-\frac{\partial \varphi_1(0,z)}{\partial x}\right)dz = \int_{-h_3}^{-h_1} \left(-\frac{\partial \varphi_3(0,z)}{\partial x} - \frac{\partial \psi_3(0,z)}{\partial z}\right)dz, \tag{36}$$

$$\int_{-h_3}^{-h_1} i\omega\rho_{water}\varphi_2(0,z)dz = \int_{-h_3}^{-h_1} \left[i\omega\rho_{ice}\varphi_3(0,z) + 2\rho_{ice}\nu_{e3}\left(-\frac{\partial^2 \varphi_3(0,z)}{\partial x^2} - \frac{\partial^2 \psi_3(0,z)}{\partial x \partial z}\right)\right]dz, \tag{37}$$

$$\int_{-h_3}^{-h_1} \rho_{ice}\nu_{e3}\left(-2\frac{\partial^2 \varphi_3(0,z)}{\partial x \partial z} - \frac{\partial^2 \psi_3(0,z)}{\partial z^2} + \frac{\partial^2 \psi_3(0,z)}{\partial x^2}\right)dz = 0, \tag{38}$$

$$\int_{-h_1}^{0} \rho_{ice}\nu_{e1}\left(-2\frac{\partial^2 \varphi_1(0,z)}{\partial x \partial z} - \frac{\partial^2 \psi_1(0,z)}{\partial z^2} + \frac{\partial^2 \psi_1(0,z)}{\partial x^2}\right)dz = \int_{-h_1}^{0} \rho_{ice}\nu_{e3}\left(-2\frac{\partial^2 \varphi_3(0,z)}{\partial x \partial z} - \frac{\partial^2 \psi_3(0,z)}{\partial z^2} + \frac{\partial^2 \psi_3(0,z)}{\partial x^2}\right)dz. \tag{39}$$

3. Solutions

In general, the full solution of the wave propagation through a viscoelastic cover consists of an infinite series of modes, each with a different wave number, all of them roots of the dispersion relation shown in Eq. (19). Truncation of this infinite series provides approximate solutions. Following Wang and Shen (2011), from solutions of Eq. (19) the two wave numbers closest to the open water case are chosen to form the approximate solution. Each of these two modes on the left side of the domain shown in Fig. 3 is represented by an incoming magnitude I. When entering the right side with a different viscoelastic property, the wave reflects in part represented by R, and transmits the rest represented by T. Thus the total potential function and the stream function may be written in terms of these two modes as follows, where the individual modes denoted by $n = 1, 2$ are given in Eqs. (12)–(14).

$$\varphi_1(x,z,t) = \sum_{n=1}^{2} I(n)(A_1(n)\cosh k_1(n)z + B_1(n)\sinh k_1(n)z)e^{ik_1(n)x}e^{-i\omega t} + \sum_{n=1}^{2} R(n)(A_1(n)\cosh k_1(n)z + B_1(n)\sinh k_1(n)z)e^{-ik_1(n)x}e^{-i\omega t}, \tag{40}$$

$$\psi_1(x,z,t) = \sum_{n=1}^{2} I(n)(C_1(n)\cosh\alpha_1(n)z + D_1(n)\sinh\alpha_1(n)z)e^{ik_1(n)x}e^{-i\omega t} + \sum_{n=1}^{2} R(n)(C_1(n)\cosh\alpha_1(n)z + D_1(n)\sinh\alpha_1(n)z)e^{-ik_1(n)x}e^{-i\omega t}, \tag{41}$$

$$\varphi_2(x,z,t) = \sum_{n=1}^{2} I(n)E_1(n)\cosh k_1(n)(z+H)e^{ik_1(n)x}e^{-i\omega t} + \sum_{n=1}^{2} R(n)E_1(n)\cosh k_1(n)(z+H)e^{-ik_1(n)x}e^{-i\omega t}, \tag{42}$$

$$\varphi_3(x,z,t) = \sum_{n=1}^{2} T(n)(A_3(n)\cosh k_3(n)z + B_3(n)\sinh k_3(n)z)e^{ik_3(n)x}e^{-i\omega t}, \tag{43}$$

$$\psi_3(x,z,t) = \sum_{n=1}^{2} T(n)(C_3(n)\cosh\alpha_3(n)z + D_3(n)\sinh\alpha_3(n)z)e^{ik_3(n)x}e^{-i\omega t}, \tag{44}$$

$$\varphi_4(x,z,t) = \sum_{n=1}^{2} T(n)E_3(n)\cosh k_3(n)(z+H)e^{ik_3(n)x}e^{-i\omega t}. \tag{45}$$

In the above,

$$\alpha_i^2(n) = k_i^2(n) - i\omega/\nu_{ei}, \quad i = 1,3 \quad \text{and} \quad n = 1,2. \tag{46}$$

The solution matrix for $A_i(n)$, $B_i(n)$, $C_i(n)$, $D_i(n)$ and the equation for solving $E_i(n)$ can be found in Appendix B. After which we can substitute the solutions of $A_i(n)$, $B_i(n)$, $C_i(n)$, $D_i(n)$, $E_i(n)$ into the horizontal boundary conditions to form nine linear equations for $I(1)$, $R(1)$, $R(2)$, $T(1)$, and $T(2)$. Since a linear wave regime is assumed, we may focus on the incoming wave one mode at a time. The procedure for solving $I(2)$ is identical. Following the above steps, substituting Eqs. (40)–(45) into Eqs. (31)–(39) gives an under-determined system of nine equations involving only five unknowns $I(1)$, $R(1)$, $R(2)$, $T(1)$, and $T(2)$. We solve this using singular value decomposition method based on the least-square error method to find the pseudo-inverse.

With the continuity condition of the vertical displacement at the interface, we can derive the transmission and reflection coefficients for the surface profile.

$$R(1) = \frac{|R(1)||k_1(1)B_1(1) + ik_1(1)C_1(1)|}{|I(1)||k_1(1)B_1(1) - ik_1(1)C_1(1)|}, \tag{47}$$

$$R(2) = \frac{|R(2)||k_1(2)B_1(2) + ik_1(2)C_1(2)|}{|I(1)||k_1(1)B_1(1) - ik_1(1)C_1(1)|}, \tag{48}$$

$$T(1) = \frac{|T(1)||k_3(1)B_3(1) - ik_3(1)C_3(1)|}{|I(1)||k_1(1)B_1(1) - ik_1(1)C_1(1)|}, \tag{49}$$

$$T(2) = \frac{|T(2)||k_3(2)B_3(2) - ik_3(2)C_3(2)|}{|I(1)||k_1(1)B_1(1) - ik_1(1)C_1(1)|}. \quad (50)$$

In the next section we will investigate several special cases for which previous results may be used for comparison.

4. Wave transmission and reflection – pure elastic covers

In this section we study the behavior of wave propagation involving pure elastic ice covers. The results are compared with existing theories. For all cases shown in this study, $\rho_{ice} = 917$ kg/m^3, $\rho_{water} = 1000$ kg/m^3, $H = 100$ m. Because $R(2)$ is very small for large shear modulus, it is dropped from the discussion in this section. $R(1)$ is denoted as R in the results shown below.

4.1. Between open water and elastic ice

We first consider the case of wave propagation from open water to an elastic ice cover. We use the formulation described in Section 2, where no limitations of the ice thickness is imposed. The transmission and reflection coefficients are defined in Eqs. (47)–(50). Fig. 4 shows the reflected and transmitted coefficients with respect to the wave period for $\nu = 0$ m^2/s, $G_1 = 0.001$ Pa, $G_3 = 5$ GPa, $h_1 = 0.001$ m, and $h_3 = 0.5$ m. Because of the extremely small values of G_1 and h_1, our solution should converge to that of the open water connecting to an elastic cover given in Wang and Shen (2011), as indeed shown in Fig. 4. In this figure, the more accurate solutions using the Eigenfunction Expansion Matching Method by Kohout et al. (2007) are also shown for comparison.

4.2. Between thin and thick elastic ice

Next we consider a case with a vanishing h_1 and a finite h_3 but keeping the same shear modulus in both ice regions. This case represents the wave propagation from an elastic membrane into an ice cover. The resulting reflection and transmission coefficients are plotted in Figs. 5 and 6. From Fig. 5, it is clear that when h_1 decreases wave transmission converges to that of the case from open water to an ice cover. However, the reflection coefficient is different. Convergence is still observed when h_1 decreases, but the results differ from the open water case except for long waves. The constitutive behavior of the membrane affects the reflection even though its thickness is negligible. This effect diminishes when the shear modulus of the membrane approaches zero, as observed earlier in Fig. 4.

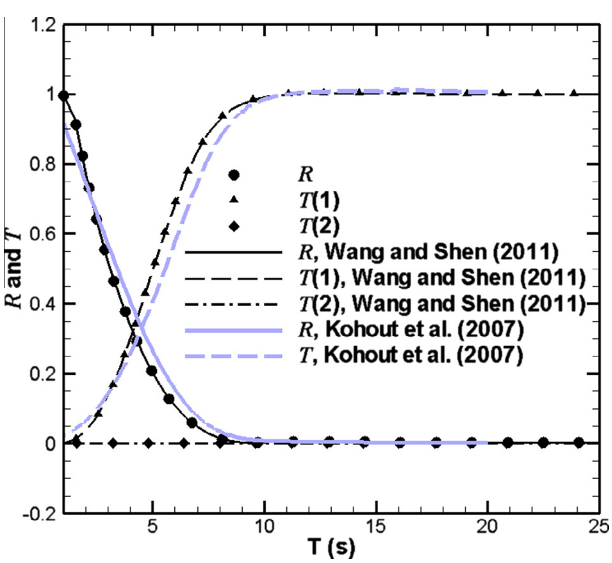

Fig. 4. Comparison between previous and the present studies of the reflection and transmission coefficients from open water to an elastic cover with respect to wave period. Here $\nu = 0$m^2/s for both regions, $G_1 = 0.001$ Pa, $G_3 = 1$ GPa, $h_1 = 0.001$ m, and $h_3 = 0.5$ m. In this and the rest of the figures, $\rho_{ice} = 917$ kg/m^3, $\rho_{water} = 1000$ kg/m^3, H = 100 m. (The dark solid line coincides with the circles. The dark dash line coincides with the triangles. The dark dash-dot line coincides with the diamonds.)

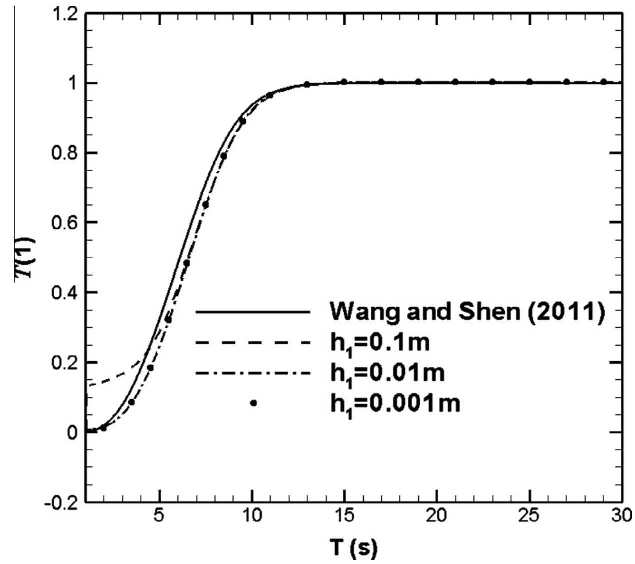

Fig. 5. Transmission coefficient with respect to wave period between a thin elastic cover and finite thickness elastic cover. Here $\nu = 0$ m^2/s for both regions, $G_1 = G_3 = 5$ GPa, $h_3 = 0.5$ m. (The dash-dot line coincides with the circles.)

4.3. Between arbitrary elastic ice covers

We now consider two linear elastic ice covers with different properties. This case has been studied by Barrett and Squire (1996) using the thin elastic plate theory. First we present the case where the shear modulus differs between the two ice regions, all other parameters are identical. The results are shown in Fig. 7. We have also tested the case where two ice regions are identical. The results show $T = 1$ and $R = 0$ for all wave periods, as expected.

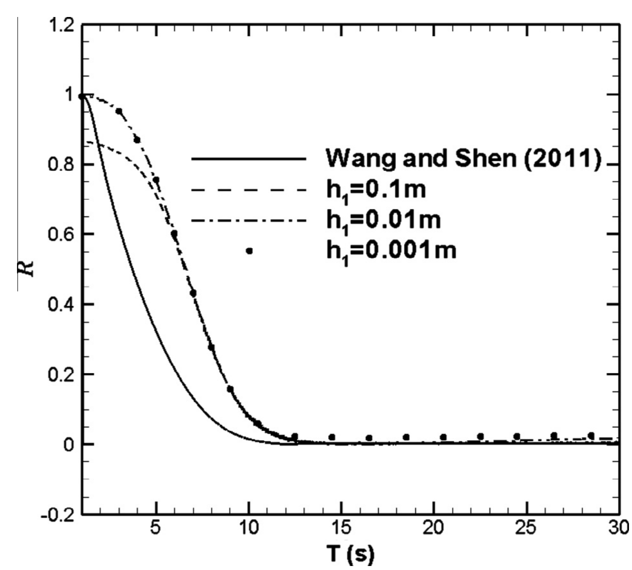

Fig. 6. Reflection coefficient with respect to wave period between a thin elastic cover and finite thickness elastic cover. Here $\nu = 0$ m^2/s for both regions, $G_1 = G_3 = 5$ GPa, $h_3 = 0.5$ m. (The dash-dot line coincides with the circles.)

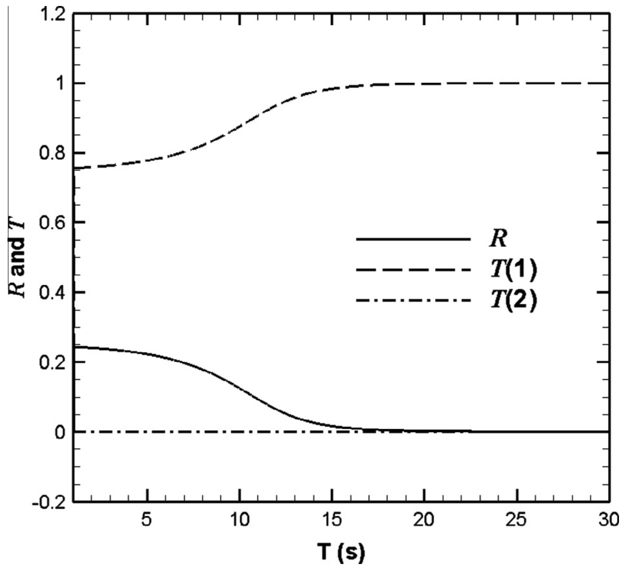

Fig. 7. Reflection and transmission coefficients with respect to wave period between two elastic ice regions with $\nu = 0\ m^2/s$ in both regions, $G_1 = 2.5$ GPa, $G_3 = 5$ GPa, and $h_1 = h_3 = 1$ m.

Next we examine the case when the ice thickness is different between the two regions, the rest of the parameters are identical. The results are shown in Fig. 8.

The above reflection and transmission coefficients are qualitatively the same as in Barrett and Squire (1996) if their smoothly joined sheet boundary conditions are used. The quantitative difference is substantial at low wave periods but diminishes at high periods. The difference is particularly noticeable for the reflection coefficient. For example, for a 1 s wave, the reflection coefficient for the case shown in Fig. 7 is about 0.05 from Barrett and Squire (1996) but from the present calculation it is about 0.25. The difference in transmission is less. For a 1 s wave, it is about 0.9 from Barrett and Squire (1996) and 0.7 from the present calculation. The differences in both reflection and transmission become negligible for long wave periods. This difference may be a combination of our approximation in treating the boundary conditions, in ignoring the evanescent modes, as well as the continuum considerations used in the ice regions (instead of the thin elastic plate assumption). Further investigation to identify the source of these differences awaits a more complete mathematical study currently underway.

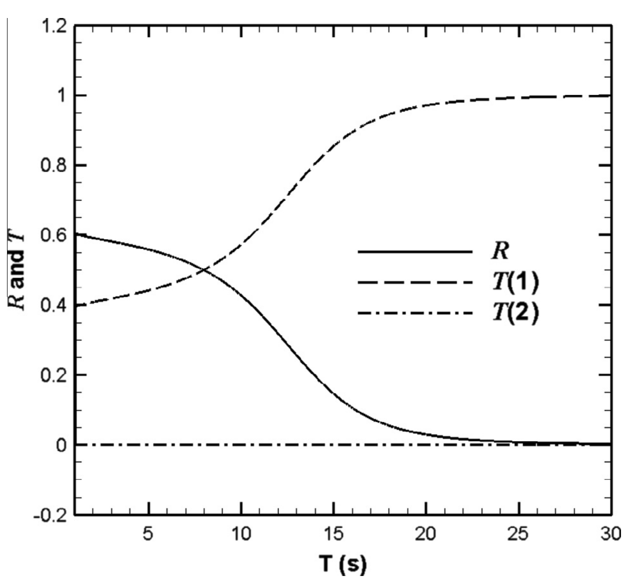

Fig. 8. Reflection and transmission coefficients with respect to wave period between two elastic ice regions with $\nu = 0\ m^2/s$ in both regions, $G_1 = G_3 = 5$ GPa, and $h_1 = 1$ m, $h_3 = 2$ m.

5. Viscoelastic cases

We next study the full viscoelastic case. Each ice region is now considered as a viscoelastic material with different properties. In this section, both $R(1)$ and $R(2)$ are included.

5.1. Between viscoelastic ice

First we examine regions of two different thicknesses. This case corresponds to an ice cover of the same physical composition but varying thickness. In each case, we let $h_1 = 1$ m, $h_3 = 2$ m. Properties in these two regions are otherwise identical. We study the influence of viscosity for three different shear moduli: low, intermediate, and high. These results are shown in Figs. 9–11, respectively. As shown in Fig. 9, for low shear modulus, over a very large range, viscosity has strong effect on the transmission and reflection coefficients. Such dependence on viscosity appears to vanish as shear modulus increases for all three cases. However, looking close at the smaller range of viscosity, as shown in the insets of each figure, a different picture is found. The viscosity effect for $0 < \nu < 1\ m^2/s$ is most pronounced for the case with highest shear modulus. In fact, upon close examination, viscosity does change the behavior of the transmission and reflection, but its influence is pushed down towards lower values of viscosity as the shear modulus grows.

5.2. Effect of shear modulus

In studying wave propagation from open water to a viscoelastic cover, a mode switching phenomenon was observed between the two modes included in the approximate solution (Wang and Shen 2011). One of the two modes having most of the transmitted energy was called the dominant mode. It was found that between open water and an elastic cover, as the shear modulus increased, the dominant mode changed from one to the other. In this section,

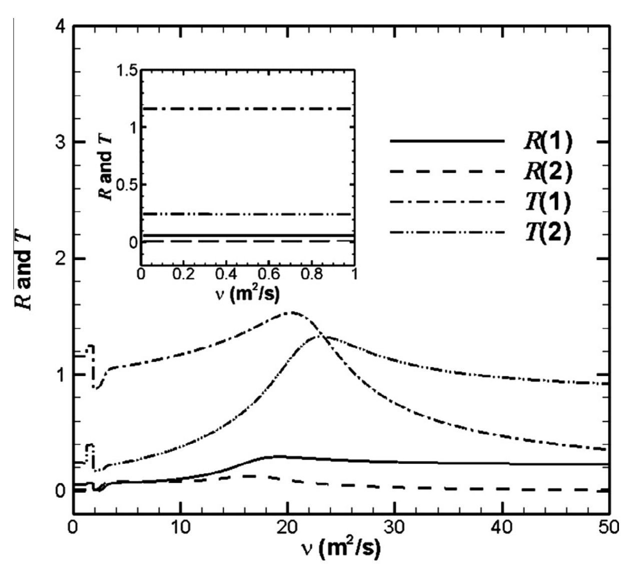

Fig. 9. Reflection and transmission coefficients with respect to viscosity between two thin elastic ice covers with T = 6 s, $G = 10^4$ Pa, and $h_1 = 1$ m, $h_3 = 2$ m.

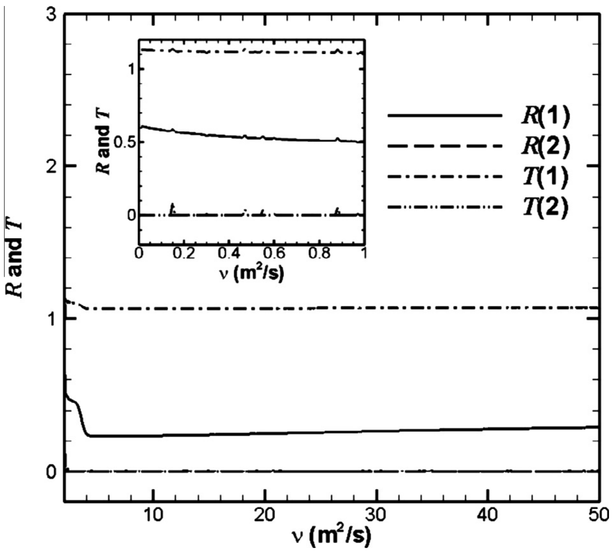

Fig. 10. The same as in Fig. 9, except that $G = 10^5$ Pa. ($R(2)$ and $T(2)$ are both very close to zero.)

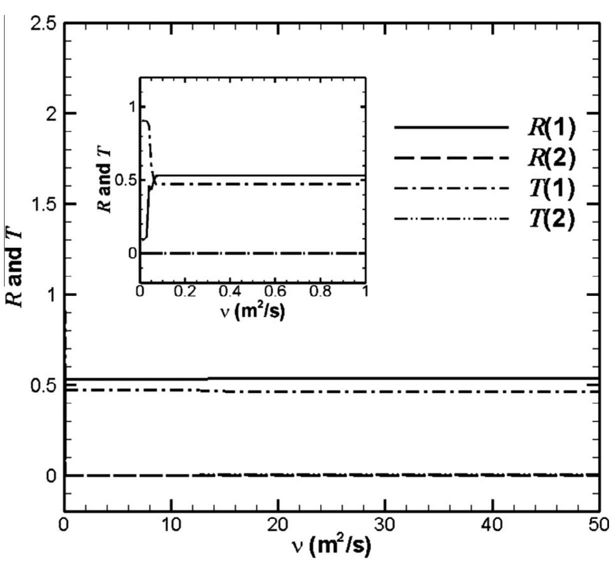

Fig. 11. The same as in Fig. 9, except that $G = 1$ GPa. ($R(2)$ and $T(2)$ are both very close to zero.)

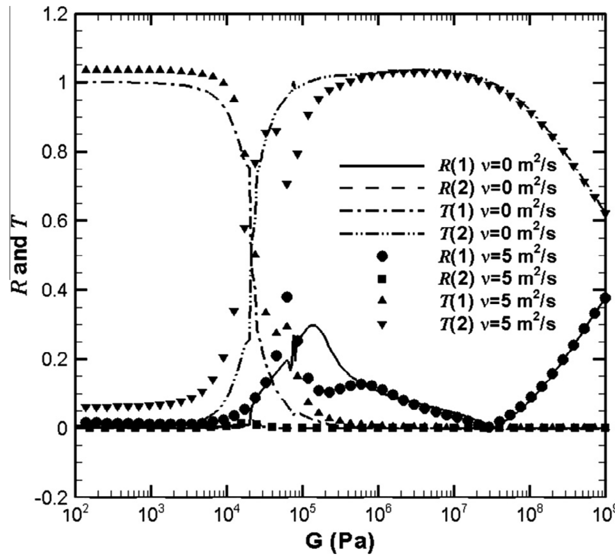

Fig. 12. Reflection and transmission coefficients between two viscoelastic ice covers with $\nu = 0\ m^2/s$ or $5\ m^2/s$, $T = 6$ s, and $h_1 = 0.1$ m, $h_3 = 0.5$ m. (Two $R(2)$ are both very close to zero.)

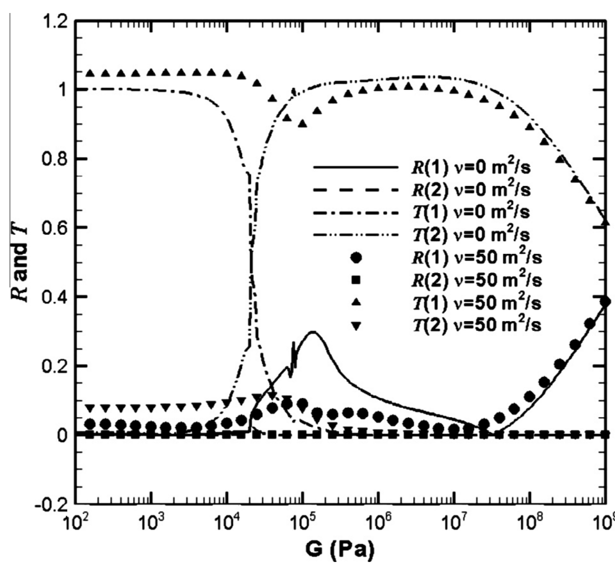

Fig. 13. The same as in Fig. 12 except that $\nu = 0\ m^2/s$ or $50\ m^2/s$. (Two $R(2)$ are both very close to zero.)

we investigate the energy partition between these two modes between viscoelastic covers. The transmission and reflection coefficients are shown in Figs. 12 and 13 for the two modes over a range of the shear modulus. Just like in the previous case between open water and an elastic cover, the mode with a greater transmission switched from one to the other in the range of $G = 10^4$–10^5 Pa. The viscosity can influence the presence of mode switching. Between $\nu = 0$ and $5\ m^2/s$, there is little difference as shown in Fig. 12. Increasing the viscosity to $50\ m^2/s$, the mode switching stops as shown in Fig. 13. Having such a large viscosity is unlikely for the ice cover. However, when considering the ice cover together with the boundary layer underneath, the full dissipation mechanism of this upper layer in the wave field may result in a large effective viscosity. Whether what found in the current model is physically observable remains to be seen.

We also tested the case when water depth is 1000 m. There is no discernible difference from the $H = 100$ m case. The insensitivity to water depth may be an artifact of the approximation, since we keep only two modes in the solution.

5.3. Grease ice and elastic ice

As mentioned in the introduction, although this study is intended for a geophysical scale model, the same analysis is also applicable to floe scale process. We thus study a relevant case here. Figs. 14 and 15 show results of a wave propagating from a pure viscous layer to a pure elastic cover. This situation corresponds to an ice floe surrounded by grease ice. We test a pure viscous case $\nu_1 = 0.01\ m^2/s$ in region 1 and let regions 3 be pure elastic. This viscosity is chosen based on the experimental study of grease ice covers (Newyear and Martin, 1999). The results are compared to the wave propagation from open water (with $\nu = 0\ m^2/s$ and $G_1 = 0$ Pa) to the same elastic cover in region 3. We choose two cases for the elastic region: an intermediate shear modulus ($G_3 = 0.05$ GPa) and a high shear modulus ($G_3 = 5$ GPa). As shown in Figs. 14 and 15, $R(2)$ is non-zero for small period, but the trans-

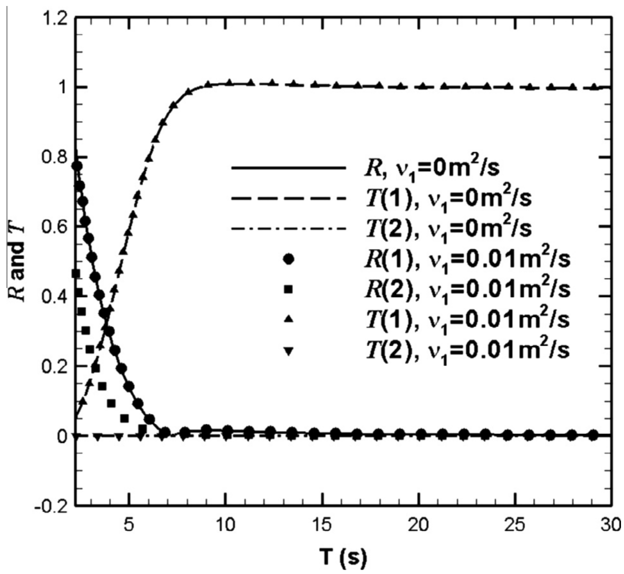

Fig. 14. Reflection and transmission coefficients with respect to wave period from open water or a pure viscous ice to a pure elastic ice with $G_1 = 0$ Pa, $\nu_1 = 0$ m^2/s or 0.01 m^2/s, $G_3 = 0.05$ GPa, $\nu_3 = 0$ m^2/s, and $h_1 = 1$ m, $h_3 = 1$ m.

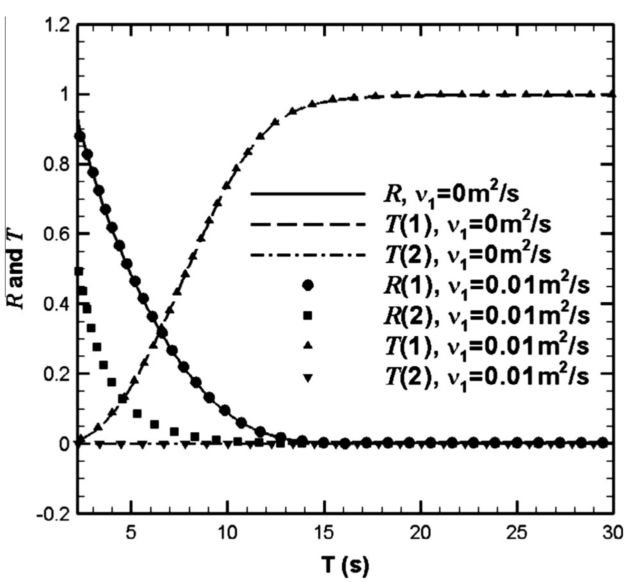

Fig. 15. The same as in Fig. 14, except that $G_3 = 5$ GPa.

mission and reflection coefficients for the dominant mode are unaffected whether it is from open water or from a grease ice layer.

6. Summary

In the present study, the approximate mode decomposition method for solving ocean wave propagating from open water to an ice-covered region is extended to two connected ice-covered regions. In each region the ice cover is modeled as a viscoelastic continuum.

6.1. Boundary conditions

The boundary conditions in the vertical direction are the same as in Wang and Shen (2010). These conditions have been used to obtain the dispersion relation. In which, the attenuation coefficient and the wavelength have been obtained. The boundary conditions in the horizontal direction included more constraints from the previous study of Wang and Shen (2011). In addition to requiring the continuity conditions of horizontal velocity and normal stress, we also consider the continuity conditions of shear stress and vertical velocity. Equivalent conditions were included by Barrett and Squire (1996) for thin elastic plate models. For ice-ice interface, we also include the vertical velocity continuity condition to achieve the non-slip boundary condition. In Wang and Shen (2011), continuity of shear stress was first included in the solution procedure. The solutions showed no influence of including this condition in the case of open water connecting to a viscoelastic cover. Hence this condition was dropped later in that study. For the present case we have kept this condition. However, because the magnitude of shear stress is proportional to the shear modulus, with its large value this constraint makes the convergence to the solution extremely difficult. To avoid the divergence of the results when solving for the reflection and transmission coefficients, we use a weighting factor of $0.1/G$ for the shear stress boundary condition when applying the singular value decomposition procedure. With this weighting factor, the solutions converge easily.

Instead of requiring a minimum overall error throughout the boundaries as in Fox and Squire (1990, 1994), we only require the mean values on both sides of the interface be the same. This approximation as adopted in Wang and Shen (2011) makes the solution procedure much simpler. Because of the approximation, results for shorter waves presented here are less accurate.

To investigate the amount of error introduce by this approximation, Fig. 16 shows the contribution of error from each of the boundary conditions in Eqs. (20)–(28). For the selected example, the parameters are $G_1 = G_3 = 5$ GPa, $\nu_1 = \nu_3 = 0$ m^2/s, $h_1 = 1$ m, $h_3 = 2$ m and $H = 100$ m. In this figure, we plot the integrals in Eq. (30) one term at a time. The behaviors of the errors can be separated into four distinct groups. The first group is the errors from Eqs. (20) and (21) for water-water interface. This group shows a fast decay with increasing period, hence they are the main error sources for low period waves. The second group is Eqs. (22), (25), and (26). These equations represent the velocity boundary conditions. This group is flat with a small magnitude, hence does not contribute significantly to error. The third group contains the normal stress terms, Eqs. (23) and (27), and the shear stress term, Eq. (28). Similar to the second group, the third group is also flat with

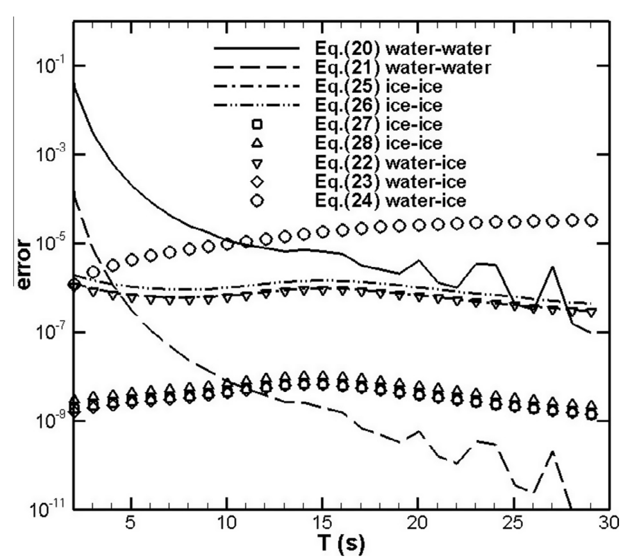

Fig. 16. Error terms from different boundary conditions: $G_1 = G_3 = 5$ GPa, $\nu_1 = \nu_3 = 0$ m^2/s, $h_1 = 1$ m, $h_3 = 2$ m and $H = 100$ m.

very small magnitude. The fourth group is from the shear stress boundary condition, Eq. (24). This error increases with increasing period, thus becomes the main error source for large periods. Of the nine boundary conditions, Eq. (24) is the most challenging. It represents the matching of shear stress between the vertical interface of water and ice. Referring to Fig. 3, this interface is below water. On the left side the shear stress must be uniformly zero due to the inviscid water. Thus the shear stress must also vanish on the ice side where it meets water. However, above the water–ice interface, still at $x = 0$, is the ice-ice interface where the shear stress is not zero. The normal stress at the same interface does not suffer this jump condition, because the continuity of normal stress between regions 1 and 2 and regions 1 and 3 helps to smoothly connect the normal stress between regions 2 and 3. Nevertheless, the increase of error from Eq. (24) with wave period is mild. Its magnitude is small even for long period waves thus should not influence the solution significantly as is evident from Fig. 4. Several other parameter ranges have been studied. The characteristics of the error terms remain the same as shown in this example.

Improvement of the solution using the variational method to solve the boundary conditions together with including more modes from the dispersion relation is underway and will be presented in the future. The errors discussed above are expected to reduce with the improved solution procedure. Partial submergence is also desired in order to more closely describe floating ice covers.

6.2. Wave transmission and reflection between two elastic covers

To compare with previously established wave transmission and reflection, we investigate the case between two elastic covers and compare the present results with the thin elastic plate model. The cases for changes on ice thickness and shear modulus between the two ice-covered regions are studied as shown in Figs. 7 and 8. We find that present results are qualitatively the same as in Barrett and Squire (1996) under their smoothly joined sheet boundary conditions. The quantitative difference may come from our ignoring the evanescent modes, keeping only two modes, and possibly our inclusion of the constitutive relation and the resulting boundary conditions between the ice regions. When we set the thickness and shear modulus of the upstream side of the ice region to zero, the results converge to open water connecting to an elastic cover as shown in Figs. 4–6.

6.3. Effect of viscosity

After validating the current formulation and solution procedure by comparing the results with previously published work, we calculate the viscoelastic case. Several interesting phenomena are found. First, the mode switching that occurs as shear modulus increases stops at very high viscosity (see Fig. 13). Interest in such phenomena is at present only academic, because no evidence of such high effective viscosity is physically possible. Second, the transmission from a pure viscous cover to an elastic cover is the same as that from open water to an elastic cover, Figs. 14 and 15. The reflection of the dominant mode is also unaffected whether it is from open water or from a viscous layer. The non-zero $R(2)$ is more pronounced for shorter waves. Solutions of the transmission and reflection are influenced by evanescent modes more for shorter waves. Hence the magnitude of $R(2)$ may change when these modes are included. When the propagation direction is reversed, i.e. from the elastic cover to open water or a viscous cover, we need to determine if the same insensitivity to open water or grease ice still holds. If so, then results from wave scattering in a dispersed floe field should apply to cases of floes dispersed in a slurry. Although not intended in this study, this result is relevant for floe scale models.

Finally, viscosity does have an effect on wave transmission and reflection when the ice cover is not pure viscous. As shown in Figs. 9–11, the influence of viscosity in a viscoelastic cover is evident.

6.4. Application of viscoelastic model in the numerical wave model

In general, wave models are based on the evolution equation of the wave spectra (Tolman, 2003)

$$\frac{DF(f,\theta,\vec{x},t)}{Dt} = S(f,\theta,\vec{x},t), \tag{51}$$

where F is the wave energy density and S is the source-sink term. At present, the effect of ice is considered via an artificial blocking of energy flux between computational cells. Specifically, the advection of energy $\vec{c}_g F$ between computational cells is modified by a "transparency" coefficient which depends on the ice concentration. In the above, $\vec{c}_g$ is the group velocity. A process-based wave-ice interaction model will improve the parameterization of the existing wave models. The viscoelastic model presented here has the ability to include the elastic characteristics of a solid ice cover and the viscous characteristics of a fragmented ice field. It also has the ability to include other damping mechanisms such as the scattering, floe-floe interactions and flexing hysteresis. The dispersion relation given in Wang and Shen (2010) provides a way to calculate $\vec{c}_g$ and S. The transmission and reflection developed in the present study provides a way to calculate the "transparency" coefficient. Instead of using ice concentration as the single parameter, the wave model will use the shear modulus and viscosity as new parameters. The advantage is that frequency-dependent damping and transmission of energy may be more realistically modeled. The challenge will be to determine the effective shear modulus and viscosity for a given ice field subject to a given wave frequency.

7. Conclusions

Motivated by providing a simple model for all types of ice cover under all wave frequencies, the present study develops the solution procedure for the transmission and reflection between two dissimilar ice covers. The ice covers are conceptually represented by two parameters: shear modulus and viscosity. For extreme cases such as grease ice, the shear modulus vanishes and the ice cover behaves as a viscous material; for a consolidated ice cover the shear modulus approaches that of the solid ice and the cover behaves as an elastic material. The infinite series of all admissible modes of the dispersion relation is truncated to two closest to the open water mode. For very large or small shear modulus, only one of these modes is significant. The other has extremely low wave number associated with near zero transmission. But for intermediate shear modulus, there is a transition phenomenon between the two modes. These phenomena have been discovered in the earlier work for wave propagation from open water into a viscoelastic ice region (Wang and Shen, 2011). In the present study, it is found that at large viscosity the mode switching phenomenon disappears. It also disappears for long period waves. The work presented here is a natural extension to the previous study of Wang and Shen (2011). The method shown may be used to prepare a numerical scheme for wave modeling under a heterogeneous ice cover. The results shown also provides evidence that at floe scale, wave scattering from elastic ice floes dispersed in a grease/brash ice field is nearly the same as those dispersed in open water. Due to the nature of the approximation, for short period waves the solutions are less accurate. Improvements will require implementing more modes and better treating the boundary conditions.

Acknowledgments

The authors would like to thank the anonymous reviewers for a number of key suggestions that have improved this study. This work is supported in part by the Office of Naval Research Grant #N00014-13-1-0294.

Appendix A. Derivations of normal stresses and shear stresses in terms of the potential and stream functions

Substitute the velocity potential and stream functions into the expressions for stresses, we get

$$\tau_{xzi} = \tau_{zxi} = \rho_{ice} v_{ei}\left(\frac{\partial u_i}{\partial z} + \frac{\partial w_i}{\partial x}\right) = \rho_{ice} v_{ei}\left(-2\frac{\partial^2 \varphi_i(x,z)}{\partial x \partial z} - \frac{\partial^2 \psi_i(x,z)}{\partial z^2} + \frac{\partial^2 \psi_i(x,z)}{\partial x^2}\right), \quad (52)$$

$$\tau_{xxi} = -p_i + 2\rho_{ice} v_{ei}\frac{\partial u_i}{\partial x} = i\omega\rho_{ice}\varphi_i(x,z) + 2\rho_{ice} v_{ei}\left(-\frac{\partial^2 \varphi_i(x,z)}{\partial x^2} - \frac{\partial^2 \psi_i(x,z)}{\partial x \partial z}\right), \quad (53)$$

$$\tau_{zzi} = -p_i + 2\rho_{ice} v_{ei}\frac{\partial w_i}{\partial z} = i\omega\rho_{ice}\varphi_i(x,z) + 2\rho_{ice} v_{ei}\left(-\frac{\partial^2 \varphi_i(x,z)}{\partial z^2} + \frac{\partial^2 \psi_i(x,z)}{\partial x \partial z}\right), \quad (54)$$

$i = 1, 3,$

$$\tau_{xzi} = \tau_{zxi} = 0, \quad (55)$$

$$\tau_{xxi} = -p_i = i\omega\rho_{ice}\varphi_i(x,z), \quad (56)$$

$$\tau_{xxi} = -p_i = i\omega\rho_{ice}\varphi_i(x,z), \quad (57)$$

$i = 2, 4.$

Appendix B. Matrix for solving $A_i(n)$, $B_i(n)$, $C_i(n)$, $D_i(n)$ and $E_i(n)$

Substituting Eqs. (12) and (13) into vertical boundary conditions, Eqs. (15)–(17), we obtain the matrix for solving the coefficients $A_i(n)$, $B_i(n)$, $C_i(n)$, $D_i(n)$ as follows.

$$\begin{bmatrix} 0 & 2ik_i^2(n) & \alpha_i^2(n)+k_i^2(n) & 0 \\ -2ik_i^2(n)Sk_i^n & 2ik_i^2(n)Ck_i^n & (\alpha_i^2(n)+k_i^2(n))C\alpha_i^n & -(\alpha_i^2(n)+k_i^2(n))S\alpha_i^n \\ N_i^n\omega & -k_i(n)g & ik_i(n)g & L_i^n \\ -M_i^n Sk_i^n + N_i^n\omega Ck_i^n & M_i^n Ck_i^n - N_i^n\omega Sk_i^n & -iM_i^n C\alpha_i^n - L_i^n S\alpha_i^n & iM_i^n S\alpha_i^n + L_i^n C\alpha_i^n \end{bmatrix} \times \begin{bmatrix} A_i(n) \\ B_i(n) \\ C_i(n) \\ D_i(n) \end{bmatrix} = \begin{bmatrix} 0 \\ 0 \\ 0 \\ 0 \end{bmatrix} \quad (58)$$

Here,

$$Sk_i^n = \sinh k_i(n)h_i, \quad (59)$$

$$Ck_i^n = \cosh k_i(n)h_i \quad (60)$$

and

$$S\alpha_i^n = \sinh\alpha_i(n)h_i, \quad (61)$$

$$C\alpha_i^n = \cosh\alpha_i(n)h_i, \quad (62)$$

$$N_i^n = \omega + 2iv_{ei}k_i^2(n), \quad (63)$$

$$M_i^n = \left(\frac{\rho_{water}}{\rho_{ice}} - 1\right)k_i(n)g - \frac{\rho_{water}}{\rho_{ice}}\frac{\omega}{\tanh(H-h_i)}, \quad (64)$$

$$L_i^n = 2v_{ei}\omega k_i(n)\alpha_i(n). \quad (65)$$

In the above, $i = 1, 3$ and $n = 1, 2$. By setting the determinant of the matrix in Eq. (58) to zero, the dispersion relation shown in Eq. (19) is obtained.

Since the ice cover is considered as a continuum, the vertical velocity at the interface between two adjacent regions must be continuous. Therefore,

$$-\frac{\partial \varphi_2}{\partial z} = -\frac{\partial \varphi_1}{\partial z} + \frac{\partial \psi_1}{\partial x} \quad \text{at } z = -h_1, \quad (66)$$

$$-\frac{\partial \varphi_4}{\partial z} = -\frac{\partial \varphi_3}{\partial z} + \frac{\partial \psi_3}{\partial x} \quad \text{at } z = -h_3. \quad (67)$$

With these relations we can obtain $E_i(n)$:

$$E_i(n) = \frac{-A_i(n)Sk_i^n + B_i(n)Ck_i^n - iC_i(n)C\alpha_i^n + iD_i(n)S\alpha_i^n}{\sinh k_i(H-h_i)} \quad i = 1, 3 \text{ and } n = 1, 2. \quad (68)$$

References

Barrett, M.D., Squire, V.A., 1996. Ice-coupled wave propagation across an abrupt change in ice rigidity, density, or thickness. J. Geophys. Res. 101 (C9), 20825–20832.
Bennetts, L.G., Squire, V.A., 2009. On the calculation of an attenuation coefficient for transects of ice-covered ocean. Proc. R. Soc. A 468 (2137), 136.
Bennetts, L.G., Peter, M.A., Squire, V.A., Meylan, M.H., 2010. A three-dimensional model of wave attenuation in the marginal ice zone. J. Geophys. Res. 115 (C12043). http://dx.doi.org/10.1029/2009JC005982.
Bennetts, L.G., Squire, V.A., 2012. Model sensitivity analysis of scattering-induced attenuation of ice-coupled waves. Ocean Modell. 45–46, 1–13. http://dx.doi.org/10.1016/j.ocemod.2012.01.002.
Dumont, D., Kohout, A., Bertino, L., 2011. A wave-based model for the marginal ice zone including a floe breaking parameterization. J. Geophys. Res. 116 (C4), C04001.
Fox, C., Squire, V.A., 1990. Reflection and transmission characteristics at the edge of shore fast sea ice. J. Geophys. Res. 95, 11629–11639.
Fox, C., Squire, V.A., 1994. On the oblique reflexion and transmission of ocean waves at shore fast sea ice. Philos. Trans. R. Soc. A 347 (1682), 185–218.
Francis, O.P., Panteleev, G.G., Atkinson, D.E., 2011. Ocean wave conditions in the Chukchi Sea from satellite and in situ observations. Geophys. Res. Lett. 38, L24610.
Keller, J.B., 1998. Gravity waves on ice-covered water. J. Geophys. Res. 103 (C4), 7663–7669.
Kohout, A.L., Meylan, M.H., Sakai, S., Hanai, K., Leman, P., Brossard, D., 2007. Linear water wave propagation through multiple floating elastic plates of variable properties. J. Fluids Struct. 23 (4), 649–663.
Lamb, S.H., 1932. Hydrodynamics. Dover, New York.
Masson, D., Leblond, P.H., 1989. Spectral evolution of wind-generated surface gravity waves in a dispersed ice field. J. Fluid Mech. 202, 43–81. http://dx.doi.org/10.1017/S0022112089001096.
Newyear, K., Martin, S., 1999. Comparison of laboratory data with a viscous two-layer model of wave propagation in grease ice. J. Geophys. Res. 104 (C4), 7837–7840.
Perrie, W., Hu, Y., 1996. Air–ice–ocean momentum exchange. Part I: Energy transfer between waves and ice floes. J. Phys. Oceanogr. 26 (9), 1705–1720.
Peters, A.S., 1950. The effect of a floating mat on water waves. Commun. Pure Appl. Math. 3, 319–354.
Squire, V.A., 2007. Of ocean waves and sea-ice revisited. Cold Reg. Sci. Tech. 49, 110–133.
Squire, V.A., Dugan, J.P., Wadhams, P., Rottier, P.J., Liu, A.K., 1995. Of ocean waves and sea ice. Annu. Rev. Fluid Mech. 27, 115–168.
Tolman, H.L., 2003. Treatment of unresolved islands and ice in wind wave models. Ocean Modell. 5, 219–231.
Wadhams, P., 1973a. The effect of a sea ice cover on ocean surface waves, Ph.D. Thesis, Univ. of Cambridge, England.
Wadhams, P., 1973b. Attenuation of swell by sea ice. J. Geophys. Res. 78 (18), 3552–3563.
Wadhams, P., Squire, V.A., Goodman, D.J., Cowan, A.M., Moore, S.C., 1988. The Attenuation rates of ocean waves in the marginal ice zone. J. Geophys. Res. 93 (C6), 6799–6818.

Wang, R., Shen, H.H., 2010. Gravity waves propagating into an ice-covered ocean: a viscoelastic model. J. Geophys. Res. 115, C06024.
Wang, R., Shen, H.H., 2011. A continuum model for the linear wave propagation in ice-covered oceans: an approximate solution. Ocean Modell. 38, 244–250.
Weitz, M., Keller, J.B., 1950. Reflection of water waves from floating ice in water of finite depth. Commun. Pure Appl. Math. 3, 305–318.
Williams, T.D., Porter, R., 2009. The effect of submergence on the scattering by the interface between two semi-infinite sheets. J. Fluids Struct. 25 (5), 777–793.
Young, I.R., Zieger, S., Babanin, A.V., 2011. Global trends in wind speed and wave height. Science 332, 451–455.